Time Series Modeling of Human Operator Dynamics in Manual Control Tasks

Daniel J. Biezad* and David K. Schmidt**

School of Aeronautics and Astronautics
Purdue University
West Lafayette, Indiana

ABSTRACT

A time-series technique is presented for identifying the dynamic characteristics of the human operator in manual control tasks from relatively short records of experimental data. Control of system excitation signals used in the identification is not required. The approach is a multi-channel identification technique for modeling multi-input/multi-output situations. The method presented includes statistical tests for validity, is designed for digital computation, and yields estimates for the frequency responses of the human operator. A comprehensive relative power analysis may also be performed for validated models. This method is applied to several sets of experimental data; the results are discussed and shown to compare favorably with previous research findings. New results are also presented for a multi-input task that has not been previously modeled to demonstrate the strengths of the method.

NOMENCLATURE

channel	one of the physical variables used to describe system behavior in the time domain (observed state)
e(t)	vehicle subsystem output vector at time "t"
f(t)	manual control vector at time "t" for pilot subsystem

* Doctoral Candidate
** Professor

$G(z)$	discrete transfer function matrix
$G_{ij}(z)$	transfer function matrix relating subsystems "i" and "j"
$G_{M,k}$	predictor matrix at lag "k", $k \leq M$
$G(M,z)$	$\sum_{k=1}^{M} G_{M,k}\, z^{-k}$
$G_{ij,k}$	element i,j in $G_{M,k}$
$G_{ij}(M,z)$	$\sum_{k=1}^{M} G_{ij,k}\, z^{-k}$
i.i.d.	independent and identically distributed random variables
k	index for lag
M	maximum order for model
m	current order in identification process
N	number of vector samples
n	number of channels
T	matrix transpose (* conjugate transpose)
T(m)	Toeplitz autocorrelation matrix for order "m" process
X(t)	joint process vector
z^{-1}	backward shift operator
$\delta(t)$	control surface command vector at time "t"
Δ	uniform sample interval in seconds
ω	frequency (rad per sec)

1. INTRODUCTION

A pilot model is a mathematical expression which balances simplicity of mathematical structure with observed empirical reality according to the purpose for which it is used. A key question always facing the aviation community has been how to develop and use these models in order to specify, design, and evaluate piloted systems[1] so that they provide efficient, proven performance while admitting the pilot "symbiotically" into the control loop[2]. The successes of describing function and optimal control models in meeting this objective are well known[3], but the identification of these models is hindered by an dependence on long data records, a priori parameter knowledge, and a precisely controlled experimental environment.

A time series approach to pilot modeling, introduced ten years ago[4], initially appeared as just another "technique"; but recent applications of time series analysis to complex multi-channel tasks[5] indicate that this

approach may work well on relatively short data records with little or no a priori parameter knowledge. Moreover, the process of modeling provides a unifying mathematical "framework" relating recent research in closed-loop multi-channel identification theory to actual laboratory or flight test data records of relatively short duration. The "framework" includes establishing model existence, applying a proven identification technique, validating the resulting model, and analyzing model properties relative to model purpose.

Early researchers using time series to model manual control behavior recognized that obtaining single or multi-channel pilot models is a doubly formidable task because of the adaptive nature of the pilot and because of the inherent loop closures in the overall system[6]. Shinners[4] and Agarwal[7], in their pioneering work for single-input,single-output (dual-channel) systems, found that simple discrete transfer functions adequately described pilot manual control output in compensatory and pursuit tasks but did not consider the theoretical question of model existence or stability. The work of Goto, based on the theoretical methods of Akaike[8] and Whittle[9], considered model "existence" questions for a two subsystem closed-loop structure[10], but these methods assume that the autocorrelation statistics for the process are known a priori.

The purpose of this paper is to provide a unifying framework for time series modeling by deriving the specific theoretical and experimental conditions required for model existence and uniqueness, to apply an identification algorithm which guarantees stability and does not require a priori statistical information, and to demonstrate the application of this identification process in case studies. The derivation of existence conditions is applicable to a three subsystem closed-loop structure which contains the two subsystem results of Goto as a special case. The derived identification algorithm is called "Normalized Predictive Deconvolution", NPD, and is a generalization of the Levinson-Wiggins-Robinson algorithm[11] and the multi- channel Maximum Entropy Spectral Estimation algorithm[12].

2. THE MODEL

The pilot-as-controller discrete linear model is shown as part of a three subsystem structure in Figure 1. The double lines represent vector

precesses from three subsystems: the vehicle, the pilot, and the flight control system. Autoregressive (Markov) noise is added to each subsystem to represent a physical disturbance[13]; that is, injected noise is a linear sum of past values plus an i.i.d. discrete "shock" or "pulse". Mathematically this representation may be concisely represented by

$$X(t) = G(z)X(t) + \Psi(t) \tag{1}$$

where X(t) is a joint process vector partitioned into subsystems as

$$X(t) = \left| f^T(t), \delta^T(t), e^T(t) \right| \tag{2}$$

G(z) is a matrix of transfer functions in terms of the shift operator "z" which may also be partitioned into a general form given by

$$G(z) = \begin{vmatrix} 0 & G_{12}(z) & G_{13}(z)=G_p(z) \\ G_{21}(z)=G_f(z) & 0 & G_{23}(z) \\ G_{31}(z) & G_{32}(z)=G_a(z) & 0 \end{vmatrix} \tag{3}$$

The injected noise, Ψ (t), is assumed both autoregressive of finite order "L" and uncorrelated between subsystems. Thus, it may be represented by the block diagonal form

$$\Psi(t) = C(L,z)\Psi(t) + \rho(t) \tag{4}$$

$$C(L,z) = \begin{vmatrix} \sum_{k=1}^{L} C_{11,k} z^{-k} & 0 & 0 \\ 0 & \sum_{k=1}^{L} C_{22,k} z^{-k} & 0 \\ 0 & 0 & \sum_{k=1}^{L} C_{33,k} z^{-k} \end{vmatrix} \tag{5}$$

$$\Psi(t) = \left| R^T(t) \ , \ V^T(t) \ , \ W^T(t) \right| \tag{6}$$

$$\rho(t) = \left| r^T(t) \ , \ v^T(t) \ , \ w^T(t) \right|_{i.i.d.} \tag{7}$$

The individual elements in Equation (3), in contrast to the finite order assumption for the noise representation, are expressible either as a ratio of discrete polynomials (transfer function) or as an infinite sequence in the delay operator z^{-1} (pulse response). Thus, between subsystems "i" and "j",

$$G_{ij}(z) = \sum_{k=1}^{\infty} G_{ij,k} \, z^{-k} \tag{8}$$

If the infinite sequence of Equation (8) is truncated at order "M", an approximation to the mathematical system of Equation (1) results which will be referred to as the joint autoregressive representation (JAR). The truncated elements of G(z) are given by

$$G_{ij}(M,z) = \sum_{k=1}^{M} G_{ij,k} \, z^{-k} \qquad \text{JAR} \tag{9}$$

By combining Equations (1), (4), and (9) the JAR may be written as

$$X(t) = G(M,z) \, X(t) + \Omega(z) \, \rho(t) \tag{10}$$

$$\Omega^{-1}(z) = \left| I - C(L,z) \right| \tag{11}$$

$$C_{ii}(L,z) = \sum_{k=1}^{L} C_{ii,k} \, z^{-k} \tag{12}$$

The joint innovations representation[14], JIR, is obtained by multiplying Equation (10) by Equation (11) and solving for X(t):

$$X(t) = A(M,z) \, X(t) + \rho(t) \tag{13}$$

$$A(M,z) = \sum_{k=1}^{M} A_{M,k} \, z^{-k} = \left| C(L,z) + G(M,z) - C(L,z)G(M,z) \right| \tag{14}$$

The block diagonal form of Equations (2) and (5) is now taken into account in the relationship between the JAR and JIR. Denoting each

subsystem of X(t) by subscript "i", Equations (13) and (14) are equivalent to

$$X_i(t) = C_{ii}(L,z)\, X_i(t) + \sum_{j=1}^{3} \left| I - C_{ii}(L,z) \right| G_{ij}(M,z)\, X_j(t) + \rho_i(t) \quad (15)$$

By comparing Equations (14) and (15) one obtains

$$C_{ii}(L,z) = A_{ii}(L,z) \quad (16)$$

$$G_{ij}(M,z) = C_{ii}(L,z)\, G_{ij}(M,z) + A_{ij}(M,z) \quad ; \; i \neq j \quad (17)$$

The JIR described by Equation (13) may also be put into the form

$$X(t) = \Gamma(M,z)\, \rho(t) \quad (18)$$

$$\Gamma(M,z) = \left| I - \sum_{k=1}^{M} A_{M,k}\, z^{-k} \right|^{-1} \quad (19)$$

The autocovariance matrix is found by post multiplying Equation (18) by the transpose of X(t) and taking the expected value:

$$R_{XX}(0) = E\left| X(t) X^T(t) \right| = \Gamma(M,z)\, P(0)\, \Gamma^*(M,z) \quad (20)$$

where

$$P(0) = E\left| \rho(t)\, \rho^T(t) \right| \quad (21)$$

The power spectral density of this process[5] is

$$\Phi_{XX}(\omega) = \left| \Gamma(M,z)\, \Delta\, P(0) \Gamma^*(M,z) \right|_{z = e^{j\omega\Delta}} \quad (22)$$

which has the property

$$\Phi_{XX}(z) = \Phi_{XX}^T(z^{-1}) = \Phi_{XX}^*(z) \quad (23)$$

An approximation to the frequency response between variables "i" and "j" may be found using

$$G_{ij}(\omega) \simeq \left| G_{ij}(M,z) \right|_{z = e^{j\omega\Delta}} \quad (24)$$

If P(0) is diagonal, the relative power in state "i" is defined as

$$P_{ii}(\omega) = \sum_{j=1}^{n} \Gamma_{ij}(\omega) \Delta P_{jj}(0)\Gamma^{*}_{ij}(\omega) \tag{25}$$

and the noise power contribution to channel "i" from the noise source in channel "j" is

$$q_{ij}(\omega) = \Gamma_{ij}(\omega) \Delta P_{jj}(0)\Gamma^{*}_{ij}(\omega)\frac{1.0}{P_{ii(\omega)}} \tag{26}$$

Thus it is shown how the JIR representation of Equation (13) may be transformed into the JAR representation of Equations (9) through (12) using the recursions of Equations (16) and (17). Once validated, the properties of the identified model may be analyzed using Equations (20) through (26). There must be assurance, however, that these model representations exist in theory, and this topic is addressed in the next section.

3. THE EXISTENCE QUESTION

The primary factors in the determination of an acceptable pilot model are suitable experimental conditions, the assumed model structure, and the identification technique. Since the harm done by a faulty experiment, simulation, or flight test permanently voids the data, the conditions required for a unique and valid model are very important.

THEOREM 1: The JIR of Eqn.(18) is unique, and there is a unique mapping between the JAR of Eqn. (10) and the JIR of Eqn.(13) providing Eqn.(23) holds for the spectral density and providing there is a delay in every path of Figure 1.

For proof see the Appendix.

THEOREM 2: Given that the transfer matrix $\Gamma(z)$ has been identified from realization set $\{X(t) \mid t<N\}$ generated by $\Gamma(z)$, necessary conditions for

$$\lim_{M,N\to\infty} \hat{\Gamma}(z)=\Gamma(z) \tag{27}$$

are

(1) The joint process X(t) is full rank

(2) There is a unique factorization

$$\Phi_{xx}(\omega) = \left| \Gamma(z) U \Lambda^{1/2} (U\Lambda^{1/2})^T \Gamma^*(z) \right|_{z=e^{j\omega\Delta}} \tag{28}$$

$$\Lambda > 0 \quad \text{and} \quad U \quad \text{Unitary} \tag{29}$$

For proof see the Appendix.

The practical implications of these theorems for flight simulations and flight tests are that sufficient noise sources be used to excite the vector process X(t), that there should be no feedforward paths which violate the requirement for a delay in each loop, and that no anticipatory loops are closed by the pilot for the same reason. Although some identification schemes allow correlated noise inputs[15], there is no way to distinguish them from feedforwards and/or anticipation. If validation tests, however, indicate a positive definite and diagonal autocorrelation matrix for the noise inputs, then there is evidence that a sufficient condition has been met for uniqueness.

To summarize, the design or test engineer should assure

(1) sufficient noise excitation in measured channels;

(2) pilot anticipation negligible (implies random or random appearing inputs;

(3) physical delays exist in each channel, including feedforward, which are significant relative to sample time;

(4) data realizations are not predominantly unstable or nonstationary;

(5) validation checks include a whiteness test for the estimated noise realizations.

4. MODEL IDENTIFICATION AND VALIDATION

Given the conditions are met for model existence, an identification scheme is desired which identifies the JIR of Equation (13) from data realization set $\{X(t) \mid t<N\}$. It is especially important that the scheme be stable (identified parameters are bounded) and not be dependent on a priori knowledge of autocorrelation statistics. The identification technique

presented here is called Normalized Predictive Deconvolution (NPD), which acts directly on the data sets and results in a stable and parsimonious JIR.

The basic principle of the NPD scheme follows that established by Wiggins and Robinson[11] who generalized Burg's[16] recursion for single-channel systems by hypothesizing a set of backward predictors given by

$$X(t) = B(M,z)\, X(t)+\rho'(t) \tag{30}$$

$$B(M,z) = \sum_{k=1}^{M} B_{M,k}\, z^{k} \tag{31}$$

$$\rho'(t) = \left| r'^{T}(t) \;,\; v'^{T}(t) \;,\; w'^{T}(t) \right|_{i.i.d.} \tag{32}$$

By post multiplying Equation (13) by $X^{T}(t-k)$ and Equation (30) by $X^{T}(t+k)$, taking expected value, and expressing the result in a block matrix form, the "normal equations" of Reference (17) result:

$$\begin{vmatrix} I & -A_{m,1} & \cdots & -A_{m,m-1} & -A_{m,m} \\ -B_{m,m} & -B_{m,m-1} & \cdots & -B_{m,1} & I \end{vmatrix} \quad T(m) = \begin{vmatrix} Q_F(m) & \cdots & 0 \\ 0 & \cdots & Q_B(m) \end{vmatrix} \tag{33}$$

where

$$T(m) = \begin{vmatrix} R_{xx}(0) & \cdots & R_{xx}(m) \\ \cdot & \cdots & \cdot \\ \cdot & \cdots & \cdot \\ \cdot & \cdots & \cdot \\ R_{xx}(-m) & \cdots & R_{xx}(0) \end{vmatrix} \tag{34}$$

$$Q_F(m) = R_{xx}(0) - \sum_{k=1}^{m} A_{m,k}\, R_{xx}(-k) \tag{35}$$

$$Q_B(m) = R_{xx}(0) - \sum_{k=1}^{m} B_{m,k}\, R_{xx}(k) \tag{36}$$

In the NPD scheme the solution to the "normal equations" is recursively generated as order "m" is incremented without knowing the autocorrelation matrices a priori. The top and bottom rows of Equation (33) are each

weighted with invertible forward and backward prediction scaling matrices $S_A(m)$ and $S_B(m)$ so that

$$\bar{A}_{m+1,i} = S_A^{-1}(m+1)\, A_{m+1,i} \quad ; \; 0 \leq i \leq m+1 \tag{37}$$

$$-\bar{A}_{m+1,0} = S_A^{-1}(m+1) \tag{38}$$

$$\bar{B}_{m+1,i} = S_B^{-1}(m+1)\, B_{m+1,i} \quad ; \; 0 \leq i \leq m+1 \tag{39}$$

$$-\bar{B}_{m+1,0} = S_B^{-1}(m+1) \tag{40}$$

To derive the forward recursion formula (the backward recursion follows analagously), the scaled bottom row of the "normal equations" is multiplied by an arbitrary but invertible matrix and added to the top row of Equation (33). Next, the order is incremented from "m" to "m+1" and the scaled results are expressed in the form

$$\begin{vmatrix} I & -\bar{A}_{m+1,1} & \cdots & -\bar{A}_{m+1,m+1} \\ -\bar{B}_{m+1,m+1} & -\bar{B}_{m+1,m} & \cdots & I \end{vmatrix} T(m) = \begin{vmatrix} Q_F(m+1) & \cdots & 0 \\ 0 & \cdots & Q_B(m+1) \end{vmatrix} \tag{41}$$

By matching the terms of Equation (41) with the previously obtained linear combination of rows the following recursion results:

$$\bar{A}_{m+1,i} = S_A^{-1}(m+1)\, S_A(m) \left| \bar{A}_{m,i} - S_A^{-1}(m)\varepsilon_F(m+1)Q_B^{-1}(m)\bar{B}_{m,m+1-i} \right| \tag{42}$$

$$Q_F(m+1) = S_A^{-1}(m+1)\, S_A(m) \left| Q_F(m) - S_A(m)\varepsilon_F(m+1)Q_B^{-1}(m)\varepsilon_B(m+1) \right| \tag{43}$$

$$\bar{B}_{m+1,i} = S_B^{-1}(m+1)\, S_B(m) \left| \bar{B}_{m,i} - S_B^{-1}(m)\varepsilon_B(m+1)Q_f^{-1}(m)S_A(m)\bar{A}_{m,m+1-i} \right| \tag{44}$$

$$Q_B(m+1) = S_B^{-1} S_B(m) \left| Q_B(m) - S_B^{-1}(m)\varepsilon_B(m+1)Q_F^{-1}(m)\varepsilon_F(m+1) \right| \tag{45}$$

where $0 \leq i \leq m+1$ in the above expressions, and where the forward and backward prediction error matrices are given by

$$\varepsilon_F(m+1) = R_{xx}(m+1) - \sum_{k=1}^{m} A_{m,m+1-k} R_{xx}(k) \tag{46}$$

$$\varepsilon_B(m+1) = R_{xx}(-m-1) - \sum_{k=1}^{m} B_{m,m+1-k} R_{xx}(-k) \tag{47}$$

By defining

$$p(m+1) = S_A^{-1}(m)\varepsilon_F(m+1)S_B^{-T}(m) \tag{48}$$

$$P_A(m+1) = I - p(m+1)p^T(m+1) \tag{49}$$

$$P_B(m+1) = I - p^T(m+1)p(m+1) \tag{50}$$

$$S_A(m+1) = S_A(m) - \varepsilon_F(m+1)S_B^{-1}(m)\varepsilon_B(m+1) \tag{51}$$

$$S_B(m+1) = S_B(m) - \varepsilon_B(m+1)S_A^{-1}(m)\varepsilon_F(m+1) \tag{52}$$

it may be shown using matrix algebra that

$$\left| P_A^{1/2}(m+1) \right|^{-1} = S_A^{-1}(m+1)\, S_A(m) \tag{53}$$

$$\left| P_B^{1/2}(m+1) \right|^{-1} = S_B^{-1}(m+1)\, S_B(m) \tag{54}$$

$$A_{m+1,i} = \left| P_a^{1/2}(m+1) \right|^{-1} \left| A_{m,i} - p(m+1)S_B^T(m)Q_B^T(m)S_B(m)B_{m,m+1-i} \right| \tag{55}$$

$$B_{m+1,i} = \left| P_B^{1/2}(m+1) \right|^{-1} \left| B_{m,i} - p^T(m+1)S_A^T(m)Q_F^{-1}(m)S_A(m)A_{m,m+1-i} \right| \tag{56}$$

If the scaling matrices of Equations (37) and (39) are chosen to be the "identity" matrix, then the classical Levinson-Wiggins-Robinson (LWR) algorithm of Reference (11) results in a normalized form. If the scaling matrices are chosen so that

$$S_A^{-1}(m) = \left| Q_F^{1/2}(m) \right|^{-1} \tag{57}$$

$$S_B^{-1}(m) = \left| Q_B^{1/2}(m) \right|^{-1} \tag{58}$$

then Equation (48) defines the Partial Autocorrelation Coefficient (PAC)[12] matrix. In addition, if the following approximations are used:

$$\hat{\rho}(m+1) = \left| R_F^{1/2}(m) \right|^{-1} R_{FB}(m) \left| R_B^{1/2}(m) \right|^{-T} \tag{59}$$

where

$$R_F(m) = \sum_{t=m+1}^{N} \mathfrak{r}_F(m,t)\, \mathfrak{r}_F^T(m,t) \tag{60}$$

$$R_{FB}(m) = \sum_{t=m+1}^{N} \mathfrak{r}_F(m,t)\, \mathfrak{r}_B(m,t-1) \tag{61}$$

$$R_B(m) = \sum_{t=m+1}^{N} \mathfrak{r}_B(m,t-1)\, \mathfrak{r}_B(m,t-1) \tag{62}$$

$$i_F(m,t) = S_A(m)\mathfrak{r}_F(m,t) = X(t) - \sum_{k=1}^{m} A_{m,k} X(t-k) \tag{63}$$

$$i_B(m,t) = S_B(m)\mathfrak{r}_B(m,t) = X(t) - \sum_{k=1}^{m} B_{m,m-k} X(t-k) \tag{64}$$

then the multi-channel Maximum Entropy Spectral Estimation algorithm of Reference (12) is obtained.

Morf, Vieira, and Kailath[18] have shown that there is a one-to-one correspondence between the PAC matrices defined above and the autocorrelation matrices for a joint stationary process; moreover, they show that the characterization theorem of stochastic processes assures PAC matrices with singular values less that unity.

To determine the order "M" at which the above recursion is stopped, a variation of the multi-channel Akaike rule[19], as modified by the recommendations of Kashyap[20], is presented here as the PAC selection criterion. This criterion assumes that, as the estimates for the PAC matrix elements becomes smaller, they become more random, thus causing the determinant to also become random. To balance this effect with a term sensitive to both order "m" and number of channels "n" , the following expression was chosen as the PAC selection rule:

$$J_p(m) = N \log |\det p(m)| + m(n)^2 \log N \qquad (65)$$

The order resulting in the "first" minimum value as order "m" is incremented is chosen for the JIR.

Validation is accomplished by testing the forward innovations for whiteness. These residuals are estimated using Equation (62) and the matrix set

$$E\left|i_F(M,t)i_F^T(M,t-k)\right| \quad ; \; t \leq N \quad ; \; 0 \leq k \qquad (66)$$

which is visually tested for whiteness over a reasonable number of lags "k". Plots of JIR statistics vs actual statistics (if available) and time histories of actual vs predicted JIR data may also be used.

Summarizing, a technique called Normalized Predictive Deconvolution has been presented to identify a stable JIR of Equation (13) without a priori knowledge of the process autocorrelation matrices shown in Equation (34). The algorithm is initialized at m=0 with

$$Q_B(0) = Q_F(0) = R_{xx}(0)$$

where Equations (60) and (63) are used to approximate $R_{xx}(0)$. The scaling matrices are then chosen, as in Equations (57) and (58) for example, then

by definition

$$\left| P_A^{1/2}(0) \right|^{-1} = S_A(0) \tag{67}$$

$$\left| P_B^{1/2}(0) \right|^{-1} = S_B(0) \tag{68}$$

and Equations (38) and (40) are used to find $\bar{A}_{m,0}$ and $\bar{B}_{m,0}$.

The PAC matrix p(1) is then computed from Equations (59) through (64), from which $P_A(1)$ and $P_B(1)$ are found using Equations (49) and (50). The new forward and backward predictors are determined from Equations (55) and (56) for m=1 and finally the value of the PAC selection rule using Equation (65) is found. If desired the order is incremented and the process repeated.

Once the JIR is identified the JAR may be determined using Equations (16) and (17). The model characteristics are then calculated using Equations (22) through (26). Case studies which demonstrate the application of this identification process and analysis are presented next.

5. MODEL ANALYSIS: CASE STUDIES

In order to demonstrate the application of the JIR identification process on actual data sets a multi-channel "piloted" simulation was accomplished in the Flight Simulation Laboratory at Purdue University. Three pilots performed lateral bank angle tracking tasks using aileron deflection inputs with and without rudder deflection inputs for assistance.

In addition to obtaining the data sets, the goal of the simulation was to obtain subjective pilot ratings and comments for three vehicle configurations. The configurations were representative of large aircraft with the dutch roll modes selected to yield level 1, 2, or 3 handling qualities as currently in military specifications[21]. Table 1 summarizes the dutch roll characteristics and the corresponding pilot ratings and comments obtained during the simulation. Approximately 25 seconds (500 points at a 20 Hz sample rate) were used for modeling from each data run which was typically 60 seconds long.

The pursuit display shown to the pilot for the three-channel simulation (channels were aileron error, aileron deflection, and rudder deflection) is shown in Figure 2. For the two-channel simulation the "ball in the window" portion of the display was masked and no rudder inputs were allowed. Note from the ratings and comments in Table 1 that there is a considerable degradation for each configuration between the two-channel and the three-channel cases. This degradation is most severe for the level 3 configuration where a lateral pilot induced oscillation (PIO) resulted when the pilots were allowed to use rudder inputs.

The commanded bank angle disturbance was a second order autoregressive process given by

$$W(t) = 1.975\ W(t-1) - 0.977\ W(t-2) + .003\ w(t) \tag{69}$$

$$w(t) = \text{ i.i.d. normal } (0,1) \tag{70}$$

The parameters of this process were experimentally determined before taking tracking data to provide a realistic and unpredictable tracking signal to the pilots.

The JIR pilot model was identified using the NPD algorithm set up to provide the special case of the multi-channel Maximum Entropy Spectral Estimation algorithm[12]. The PAC order selection rule of Equation (65) consistently resulted in M=4 in Equation (13) except for the three-channel Configuration 3 where the order was M=7. Figure 3 illustrates the behavior of the PAC selection rule versus order for this case.

A typical experimental versus identified-model time history for the rudder deflection signal is shown in Figure 4 for models identified from 100, 200, and 500 points. The 100 point model used every fourth point of the data set between points 1 and 400; the 200 point model used every other point between points 1 and 400. Thus the final five seconds of the time history shows actual and predicted time histories which are independent of the modeling process. The 500 point model shows the best visual agreement between actual and predicted time histories.

The top row of the "normal equations" from Equation (33) may be used to define the predicted autocorrelation matrix as a function of lag for the identified JIR. With aileron deflection and aileron error as channels 1 and 2, respectively, the actual versus predicted autocorrelation matrix is shown in Figure 5 for the two-channel Configuration 3 , where the actual

value was estimated from the data sets using

$$R_{xx}(k) = E\left|X(t)X^{T}(t-k)\right| \tag{71}$$

The normalized residual matrix from Equations (63) and (66) is shown in Figure 6. Normalization implies that each element is divided by the square root of the products of the respective diagonal element magnitudes, or

$$\text{NORMALIZED}(i,j) = \frac{\text{ELEMENT}(i,j)}{\sqrt{\left|\text{ELEMENT}(i,i)\right|\left|\text{ELEMENT}(j,j)\right|}} \tag{72}$$

The prediction capability demonstrated in Figures 4 through 6 was typical for all identified models and was used as a validation check for all configurations. From these results it was assumed that the models passed the validation checks using experimental data.

If a model passes a validation check, the relative power analysis described by Goto[5] may be accomplished. The total power (variance) in the pilot's aileron deflection signal, computed from Equation (25), versus frequency for each two-channel configuration may be seen in Figure 7. Note that the power spectral density peak magnitude, in general, increases for configurations with higher (worse) pilot rating. Thus there is an indication that pilot workload (as evidenced by power spectral density) increases across a portion of pilot bandwidth as pilot rating increases for different configurations. This is consistent with workload being correlated with deflection rate[22].

Using Equation (26) it is possible to calculate the amount of power due to the noise source in each channel. The noise contribution versus frequency for the aileron channel is shown in Figure 8 for the two-channel Configuration 3 (the other configurations showed similar results). Note that the command disturbance noise is the primary contributor to pilot aileron deflection at low frequencies (below 3 rad/sec) and pilot injected noise (remnant) is the primary contributor to pilot aileron deflection at the higher frequencies (above 6 rad/sec). The two-channel results are summarized in Table 2 and the three-channel results are summarized in Table 3. As expected, the error variance, or element (2,2) in columns 2 and 5 of

Table 3, increases both with pilot rating and with the added workload of the three-channel task (as measured by the spectral density).

For the three-channel case studies, the total power in the pilot's aileron deflection signal for each configuration is shown in Figure 9. As in the two-channel ease study, the power spectral density peak magnitude increases for configurations with the higher (worse) rating, suggesting a proportional increase in pilot workload.

It is noted that the peak power tends to occur at the dutch roll frequency for each configuration, indicating that this mode is clearly present if not dominant in the pilot's output. If this is the case this mode may be a contributing cause to the lateral PIO occurring for Configuration 3 (refer to Table 1 for comments).

The plots depicting noise contributions into the aileron and rudder deflection signals are shown in Figures 10 and 11. In addition to the large increase in peak spectral density of Configuration 3 over the other configurations, note that command disturbance noise is not dominant in the frequency range of maximum power as in the two-channel case (Figure 8). In the aileron deflection channel, pilot injected noise contribution exceeds the command disturbance noise contribution. This same trend is even more noticeable in the noise contribution plots for the rudder channel in Figure 11, where the primary noise source is clearly pilot injected noise into the rudder channel.

To summarize the data analysis of the identified models, there is evidence that the cause of the PIO and resultant poor pilot rating is self-induced coupling caused by rudder excitation of a dutch roll mode with level 3 flying qualities. Recall in the two-channel case study for Configuration 3 that no lateral PIO occurred when the rudder input was denied the pilot. The command disturbance in each case was identically provided using Equation (69).

The frequency response of the pilot model, obtained from the approximation of Equation (24), is shown for each configuration for the three-channel cases in Figures 12 and 13. Note that for for poorly rated Configuration 3 that pilot aileron deflection is out of phase at low frequencies with displayed bank angle error.

As seen from the JIR analysis, the amount of information from the identification, validation, and analysis of models obtained from actual

data sets is very large. Thus selectivity in analysis is essential, and the purpose of the modeling effort is paramount in this selection process.

6. CONCLUSIONS

The fundamental conclusion from this research effort is that time series models and the analytical analysis tools they provide have the ability to quantitatively evaluate pilot-in-the-loop situations by displaying key relationships affecting the stability and response of a multi-channel "piloted" dynamic system. The NPD algorithm, in conjunction with the PAC selection rule, results in a parsimonious and stable multi-channel time series JIR model. This representation is unique if the existence conditions of Theorems 1 and 2 are met. Experimentally this requires sufficient and random-appearing excitation, physical delays in each path, and data realization sets which are stable.

Analysis of case studies illustrated the application of the modeling process, and demonstrated how the dominant source of a lateral PIO may be identified using analysis tools presented in this paper. It is important to remember that the case study results were primarily intended to illustrate the "application" of the identification process as opposed to a comprehensive evaluation of particular vehicle configurations.

It is recommended that the joint innovations identification process be applied to a more varied data base, including actual flight test data and flight control system variations. Multi-channel applications which study manual control response of operators in training status may also be accomplished.

7. ACKNOWLEDGMENT

The authors express their gratitude to Mr. Yuan Pin-Jar and to Capt William Smith, USAF, who are responsible for the laboratory computer programs and display setup used in the simulations, and to Mr. Chuck Malmsten for assistance in computer operation, maintenance, and data retrieval. This research was partially supported by NASA Dryden Flight Research Facility/Ames Research Center under grant no. NAG4-1. This support is appreciated.

8. APPENDIX

PROOF OF THEOREM 1. From Equation (10) we have

$$X(t) = \left|I - G(M,z)\right|^{-1} \Omega(z)\rho(t) \tag{A.1}$$

First the unique mapping between Equations (A.1) and (13) and (18) will be given, then the uniqueness conditions for the identified $\Gamma(z)$ will be derived. Referring to Figure 1 and temporarily eliminating notation for arguments let

$$K_1 = (I - G_p G_a G_f) \tag{A.2}$$
$$K_2 = (I - G_f G_p G_a) \tag{A.3}$$
$$K_3 = (I - G_a G_f G_p) \tag{A.4}$$

Expand the subsystem blocks in Equation (18) to obtain

$$X(t) = \begin{vmatrix} \Gamma_{11}(z) & \Gamma_{12}(z) & \Gamma_{13}(z) \\ \Gamma_{21}(z) & \Gamma_{22}(z) & \Gamma_{23}(z) \\ \Gamma_{31}(z) & \Gamma_{32}(z) & \Gamma_{33}(z) \end{vmatrix} \rho(t) \tag{A.5}$$

Use direct substitution from Equation (A.1) and match entries with Equation (A.5) to obtain

$$\Gamma_{11} = K_1^{-1}\Omega_{11} \tag{A.6}$$
$$\Gamma_{12} = K_1^{-1}G_p G_a \Omega_{22} \tag{A.7}$$
$$\Gamma_{13} = K_1^{-1}G_p \Omega_{33} \tag{A.8}$$
$$\Gamma_{21} = K_2^{-1}G_f \Omega_{11} \tag{A.9}$$
$$\Gamma_{22} = K_2^{-1}\Omega_{22} \tag{A.10}$$
$$\Gamma_{23} = K_2^{-1}G_f G_p \Omega_{33} \tag{A.11}$$
$$\Gamma_{31} = K_3^{-1}G_a G_f \Omega_{11} \tag{A.12}$$
$$\Gamma_{32} = K_3^{-1}G_a \Omega_{22} \tag{A.13}$$
$$\Gamma_{33} = K_3^{-1}\Omega_{33} \tag{A.14}$$

Since Ω_{ii} are non-singular prewhitening filters, K_i singular implies $\Phi_{xx}(\omega)$ singular from Equation (22). The reverse mapping is provided by the recursive relations in Equations (16) through (17). Note that if only two subsystems are present that Equations (A.6) through (A.14) yield the same

relationships given by Anderson[10] and Goto[5].

The final step in the proof is to show the uniqueness of $\Gamma(z)$ and this will be done using the following result from Popov as communicated by Anderson[10]:

For a nonsingular

$$\Phi_{xx}(z) = \Phi_{xx}^{*}(z) \tag{A.15}$$

there exists $D(z)$ such that

$$D^{*}(z)D(z) = \Phi_{xx}(z) \tag{A.16}$$

$$\det \left| D \right|_{z} = 1 > 0 \tag{A.17}$$

and there exists

$$\Phi_{xx}(\omega) = \left| \Gamma(z) \; \Delta \; P(0)\Gamma^{*}(z) \right|_{z = e^{j\omega\Delta}} \tag{A.18}$$

with $\Gamma(z)$ and $P(0)$ unique

$$\Gamma(z=\infty) = I \quad \text{and} \quad P(0) > 0 \tag{A.19}$$

To apply this result to the JAR use the condition that there is a delay in every path, thus

$$\left| G_{ij} \right|_{z=\infty} = 0 \tag{A.20}$$

$$\left| C_{ii} \right|_{z=\infty} = 0 \tag{A.21}$$

Substituting Equation (A.20) into Equations (A.6) through (A.14), and substituting Equation (A.21) into Equations (11) and (12), we obtain

$$\left| \Gamma_{ij} \right|_{z=\infty} = 0 \tag{A.22}$$

$$\left| \Gamma_{ii} \right|_{z=\infty} = I \tag{A.23}$$

$$\left| \Omega_{ii} \right|_{z=\infty} = I \qquad \text{(A.24)}$$

Thus Equation (A.19) is satisfied for the JAR. By the i.i.d. properties of $\rho(t)$, $P(0)$ is positive definite; and by the properties of a Toeplitz Autocorrelation[17] matrix

$$\Phi_{xx}(z) = \Phi^{*}_{xx}(z)$$

satisfying Equation (A.15). Therefore Popov's result applies and $\Gamma(z)$ and $P(0)$ are unique. Note that Anderson[10] has also shown that the block diagonals of $\Gamma_{ii}(z)$ must be nonsingular.

PROOF OF THEOREM 2. To prove that the joint process must be full rank for unique identification use Equation (28)

$$\Phi_{xx} = \left| \Gamma(z) \; \Delta \; P(0)\Gamma^{*}(z) \right|_{z=e^{j\omega\Delta}}$$

together with

$$R_{xx}(0) = E\left| X(t)X^{T}(t) \right| = \Gamma(z) \; \Delta \; P(0)\Gamma^{*}(z) \Big|_{z=1}$$

If $X(t)$ is less than full rank then a singular $P(0)$ is implied. A singular $P(0)$ makes one or more blocks of $\Gamma(z)$ arbitrary.

To prove the unique factorization is a necessary condition for unique identification use Equation (22) and the fact that $P(0)$ is positive definite. Then there is a unitary transformation[23] such that for some diagonal $\Lambda(0)$

$$P(0) = U\Lambda(0)U^{T} \quad , \quad \Lambda(0) > 0 \qquad \text{(A.25)}$$

Therefore

$$\Phi_{xx}(\omega) = \left| \Gamma(z)U\Delta\Lambda(0)U^{T}\Gamma^{*}(z) \right|_{z=e^{j\omega\Delta}} \qquad \text{(A.26)}$$

If $P(0)$ is not diagonal, then the identified $\Gamma(z)$ is

$$\hat{\Gamma}(z) = \Gamma(z) \; U \qquad \text{(A.27)}$$

where unitary matrix "U" depends on the correlation in $P(0)$, and thus may not be unique. If $P(0)$, however, is diagonal then $P(0) = \Lambda(0)$, $U = I$, and

$$\lim_{M,N\to\infty} \Gamma = \Gamma(z)\, U = \Gamma(z) \qquad (A.28)$$

Thus if the unitary matrix "U" is identity then a sufficient condition exists for the factorization to be unique. The "physically realizable" normalized minimum phase stable factor results as defined by Anderson[10].

9. REFERENCES

1. Onstott E., Faulkner,"Prediction,Evaluation, and Specification of Closed Loop and Multiaxis Flying Qualities",AFFDL-TR-78-3, Wright-Patterson AFB,Ohio, Feb 1978.
2. Frosch, R.,"Robots and People", Aeronautics and Astronautics, Vol 21, No. 7, pp. 34-36, Aug. 1983.
3. Rouse W.,Systems Engineering Models of Human-Machine Interaction, North Holland,1980.
4. Shinners S.,"Modeling of Human Operator Performance Utilizing Time Series Analysis",IEEE Tansactions on SMC,Vol SMC-4,No 5, pp 446-458,Sept 74.
5. Goto N.,"A Statistical Method Applied to Pilot Behavior Analysis in Multiloop Systems,"AIAA Journal of Guidance and Control, Vol 3, No 1, Jan-Feb 80, pp 62-68.
6. Willsky A.,"Relationships Between Digital Signal Processing and Control and Estimation Theory",Proceedings of the IEEE,Vol 66, No 9,Sept 78.
7. Agarwal G., Gottlieb G., Osafo-Charles F., O'Niell W., "Application of Time-Series Modeling to Human Operator Dynamics",IEEE Transactions on Systems,Man, and Cybernetics,Vol SMC-10,No 12,pp849-860, Dec 1980.
8. Akaike, H.,"On the Use of a Linear Model for the Identification of Feedback Systems",Ann. Inst. Statist. Math.,,Vol.20, 1968,pp 425-439.
9. Whittle P.,"On the Fitting of Multivariate Regressions,and the Approximate Canonical Factorization of the Spectral Density Matrix", Biometrika,Vol 50,pp129-134,1963.
10. Anderson B.D.O., Ng T.S., Goodwin G.C., "Identifiability of MIMO Linear Dynamic Systems Operating in the Closed Loop", Automatica, Vol 13, 1977, pp477-485.
11. Wiggins R.,Robinson E.,"Recursive Solution to the Multichannel Filtering Problem", Journal of Geophysical Research, Vol. 70, 1965, pp.

1885-1891.

12. Morf M.,Vieira A.,Lee D.,Kailath T.,"Recursive Multi Channel Maximum Entropy Spectral Estimation",IEEE Transactions on Geo Electronics,Vol GE-16,pp 85-94,Apr 78.
13. Gelb A.,Applied Optimal Estimation,MIT Press,Cambridge,Mass.,1974.
14. Caines P.,Chan C.,"Feedback Between Stationary Stochastic Processes", IEEE Transactions on Automatic Control, Vol AC-20, Aug 75, pp 498-508.
15. Vorchik V.,Fetisov V.,Shteinberg E.,"Identification of a Closed-loop Stochastic System",Automatika,No 7,pp41-52,July73.
16. Anderson N.,"On the Calculation of Filter Coefficients for Maximum Entropy Spectral Analysis", Geophysics, Vol. 39, No. 1, Feb 74, pp 69-72.
17. Kailath T.,"A View of Three Decades of Linear Filtering Theory", IEEE Transactions on Information Theory,Vol IT-20,pp145-181, Mar 1974.
18. Morf M.,Vieira A.,Kailath T.,"Covariance Characterization by Partial Autocorrelation Matrices", Annals of Statistics, Vol 6, No 3, pp 643-648,May 1978.
19. Akaike, H.,"Canonical Correlation Analysis of Time Series and the Use of an Information Criterion", System Identification: Advances and Case Studies, Mehra ed., Academic Press, 1976.
20. Kashyap,"Inconsistency of Akaike Rule",IEEE Transactions on Automatic Control,Vol AC-25,No 5, Oct 1980,pp 997.
21. "Military Specification-Flying Qualities of Piloted Airplanes", MIL-F-8785C, 1980.
22. Schmidt D.K., "On the Use of the OCM Objective Function as a Pilot Rating Metric", 17th Annual Conference on Manual Control, UCLA, Los Angeles, June, 1981.
23. Strang G.,Linear Algebra, Academic Press, 1978.

Table I. Three-channel case study configurations

Configuration (Level)	Dutch Roll Parameters		PR	Comments
	ξ	ω_N		
1: two-ch	0.4	2.02	2	"Responsive and predictable"
1: three-ch	--	--	4	"Some coupling from rudder in to aileron axis, but mostly well behaved"
2: two-ch	0.1	2.02	4-5	"Some oscillations and overshoots when aggressive"
2: three-ch	--	--	7	"Coupled overshoots between rudder and aileron and bank angle when aggressive; unpredictable and oscillatory bank angle made worse when aggressive on rudder."
3: two-ch	.02	4.0*	6	"Overshoots and residual oscillations;" "unpredictable;" complex aileron inputs required for control"
3: three-ch	--	--	9	"Closed loop unstable for task;" "excessive lateral PIO."

*This is the frequency of the lateral PIO

Table 2 Two-channel case study results summary

Configuration (Level)	PR	Bank Angle Error Variance deg^2	Ail. Def. Variance deg^2	Cross Covariance Bank Angle to Aileron Deflection deg^2	Maximum PSD Value of Aileron Deflection $deg^2/rad/sec$
1	2	20.9	5.3	8.2	2.2
2	4-5	32.1	6.6	11.4	2.9
3	6	77.1	11.4	20.8	3.8

Table 3 Covariance matrix summary and comparison

Configuration (Level)	2-ch Covariance Matrix $R_{xx}(0)$	* Order M	Pilot Rating PR	Three-channel Covariance Matrix $R_{xx}(0)$ [equation (4.43)]	Normalized P(0) Matrix [equation (4.44)]
1	$\begin{matrix} \delta_a & e_a \end{matrix}$ $\begin{bmatrix} 5.3, & 8.2 \\ 8.2, & 20.9 \end{bmatrix}$	4	4	$\begin{matrix} \delta_a & e_a & \delta_r \end{matrix}$ $\begin{bmatrix} 4.93, & 8.55, & 8.83 \\ 8.55, & 53.44, & 23.96 \\ 8.83, & 23.96, & 25.0 \end{bmatrix}$	$\begin{matrix} \delta_a & e_a & \delta_r \end{matrix}$ $\begin{bmatrix} 1.0, & -0.10, & 0.15 \\ -0.10, & 1.0 & 0.08 \\ 0.15, & 0.08, & 1.0 \end{bmatrix}$
2	$\begin{matrix} \delta_a & e_a \end{matrix}$ $\begin{bmatrix} 6.6, & 11.4 \\ 11.4, & 32.1 \end{bmatrix}$	4	7	$\begin{matrix} \delta_a & e_a & \delta_r \end{matrix}$ $\begin{bmatrix} 19.71, & 24.3 , & 22.46 \\ 24.3 , & 138.1 , & 43.87 \\ 22.46, & 43.87, & 34.17 \end{bmatrix}$	$\begin{bmatrix} 1.0 , & 0.11, & 0.15 \\ 0.11, & 1.0 , & 0.11 \\ 0.15, & 0.11, & 1.0 \end{bmatrix}$
3	$\begin{matrix} \delta_a & e_a \end{matrix}$ $\begin{bmatrix} 11.4, & 20.8 \\ 20.8, & 77.1 \end{bmatrix}$	7	9	$\begin{matrix} \delta_a & e_a & \delta_r \end{matrix}$ $\begin{bmatrix} 11.69, & 15.62, & 8.21 \\ 15.62, & 541.1 , & 41.78 \\ 8.21, & 41.78, & 30.5 \end{bmatrix}$	$\begin{bmatrix} 1.0 & - .19 , & .017 \\ - .19 , & 1.0 , & .011 \\ .017, & .011, & 1.0 \end{bmatrix}$

*order obtained for PAC selection rule

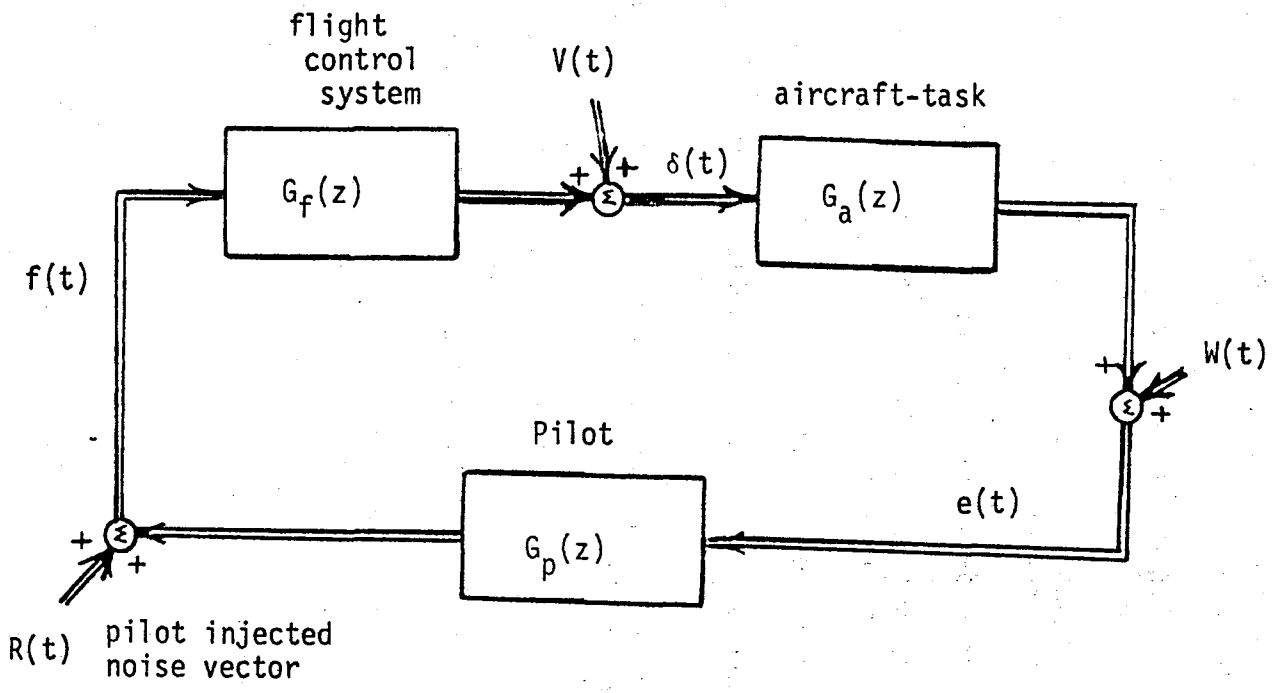
flight
control
system
$G_f(z)$
V(t)
+
+
Σ
δ(t)
aircraft-task
$G_a(z)$
f(t)
W(t)
+
Σ
+
Pilot
e(t)
$G_p(z)$
+
Σ
+
R(t)
pilot injected
noise vector

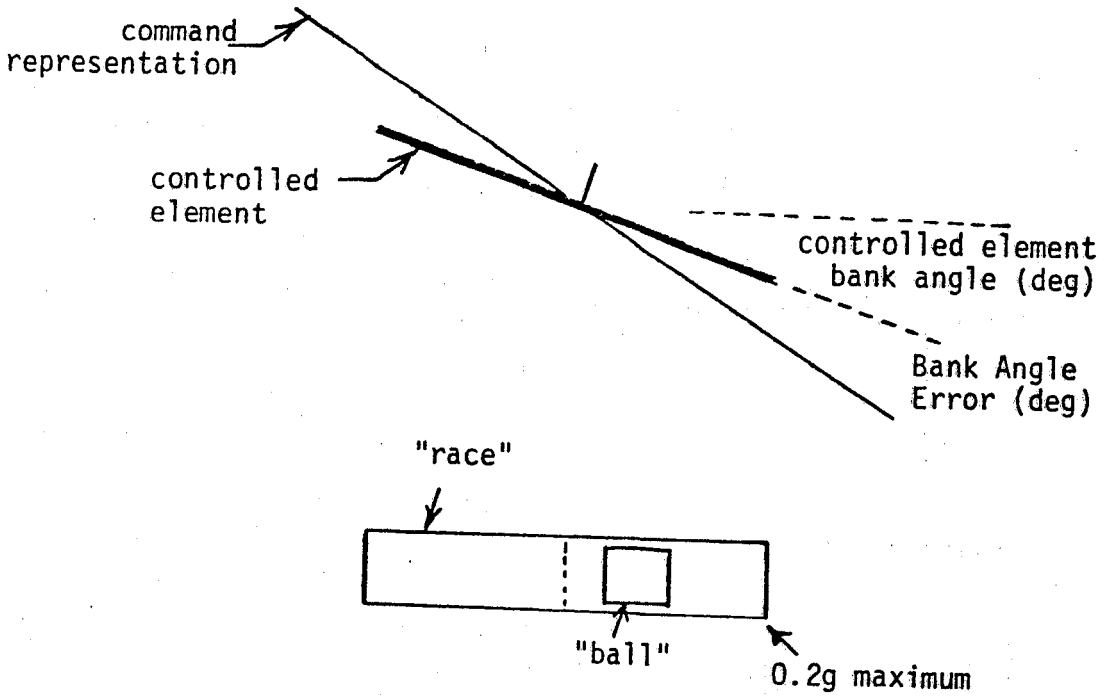
command
representation
controlled
element
controlled element
bank angle (deg)
Bank Angle
Error (deg)
"race"
"ball"
0.2g maximum

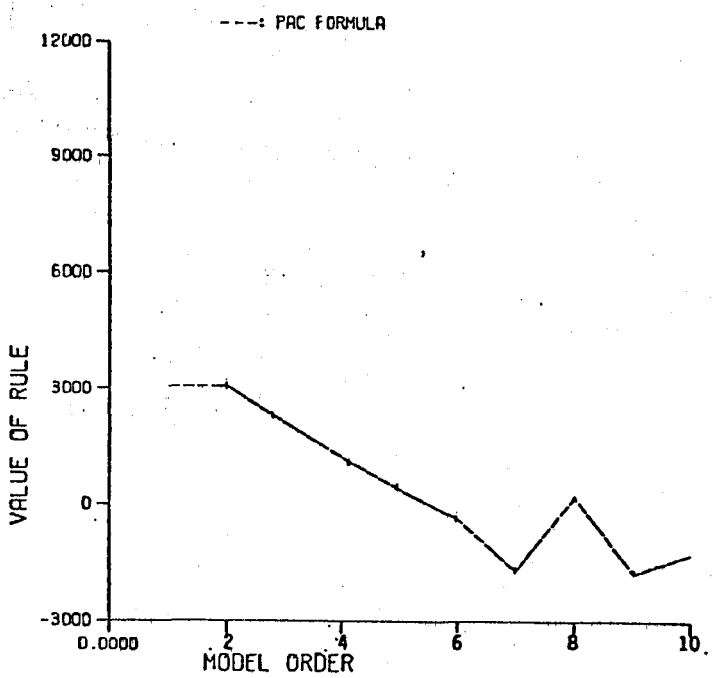
---: PAC FORMULA
12000
9000
6000
3000
0
-3000
VALUE OF RULE
0.0000
2
4
6
8
10
MODEL ORDER

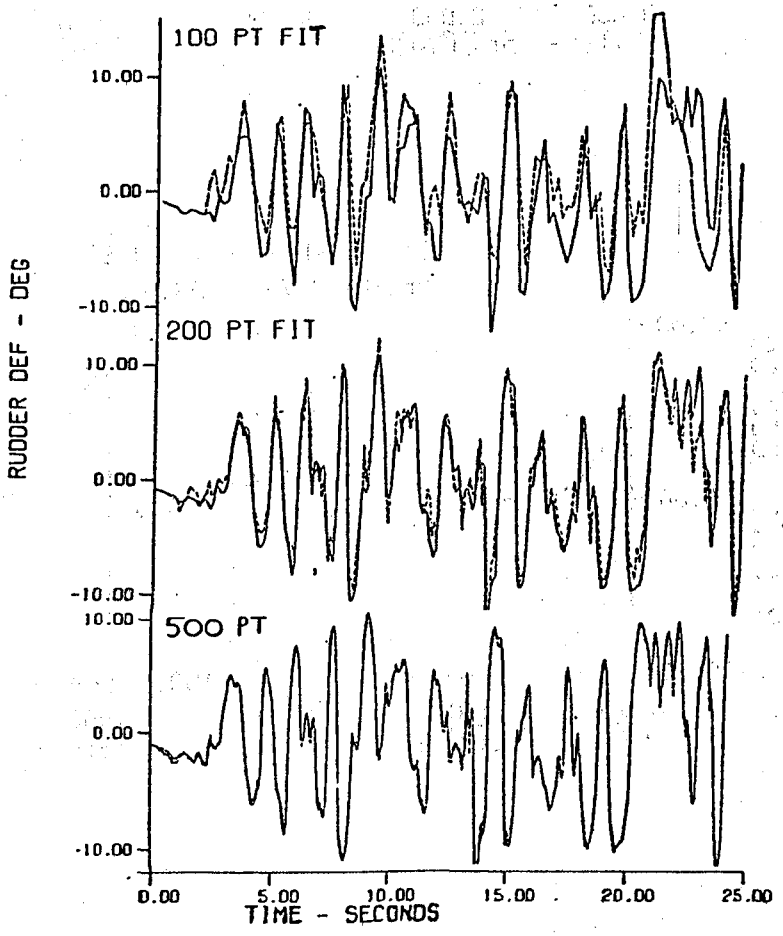
100 PT FIT
200 PT FIT
500 PT
10.00
0.00
-10.00
RUDDER DEF - DEG
0.00
5.00
10.00
15.00
20.00
25.00
TIME - SECONDS

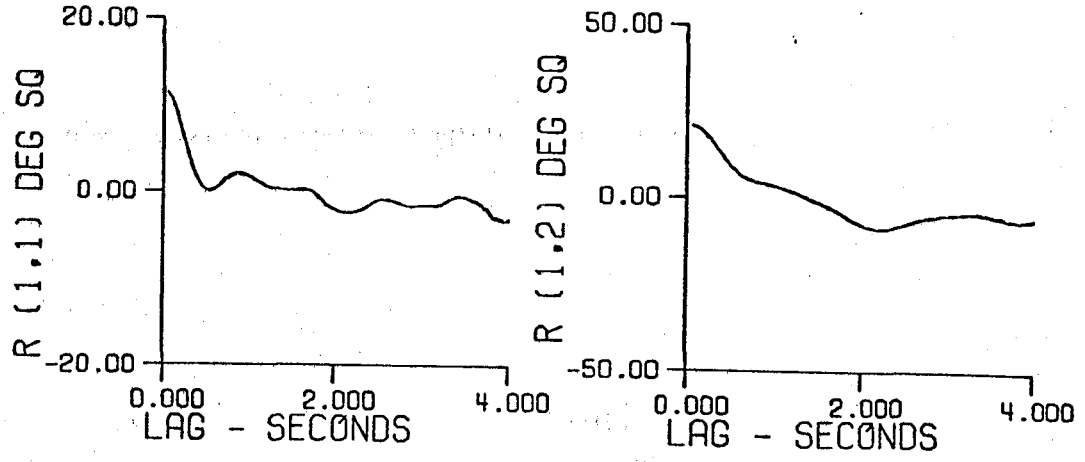
20.00
0.00
-20.00
R (1,1) DEG SQ
0.000
2.000
4.000
LAG - SECONDS
50.00
0.00
-50.00
R (1,2) DEG SQ
0.000
2.000
4.000
LAG - SECONDS

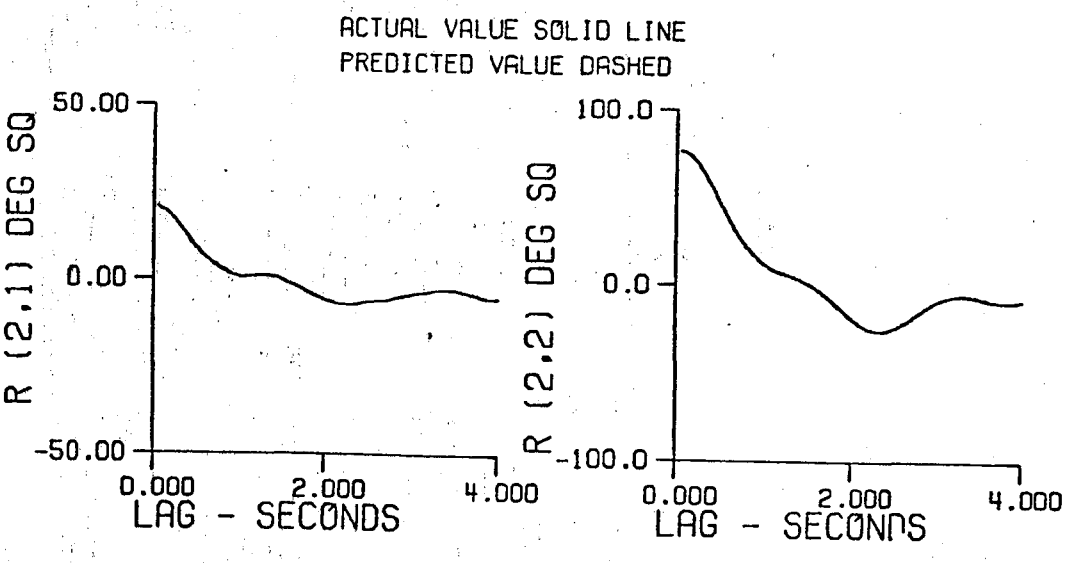
ACTUAL VALUE SOLID LINE
PREDICTED VALUE DASHED
50.00
0.00
-50.00
R (2,1) DEG SQ
0.000
2.000
4.000
LAG - SECONDS
100.0
0.0
-100.0
R (2,2) DEG SQ
0.000
2.000
4.000
LAG - SECONDS

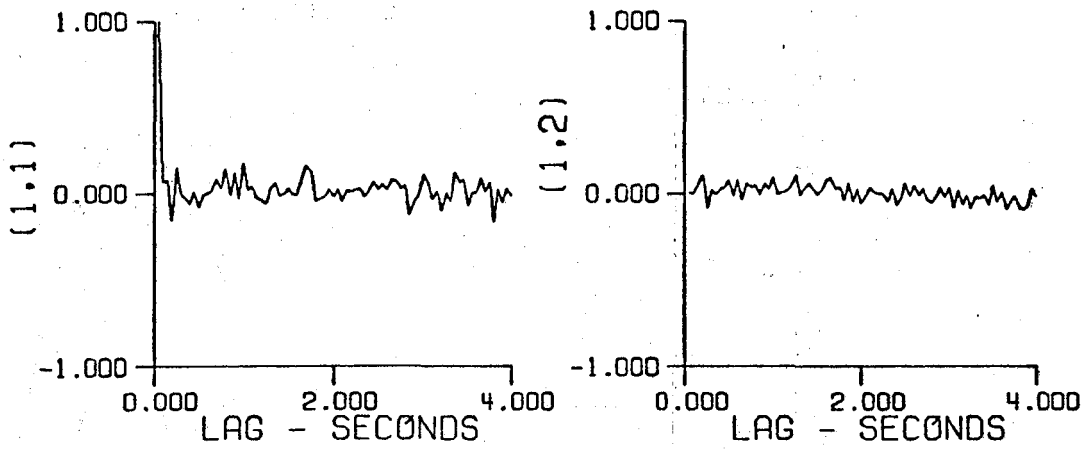
1.000
0.000
-1.000
(1,1)
0.000
2.000
4.000
LAG - SECONDS
1.000
0.000
-1.000
(1,2)
0.000
2.000
4.000
LAG - SECONDS

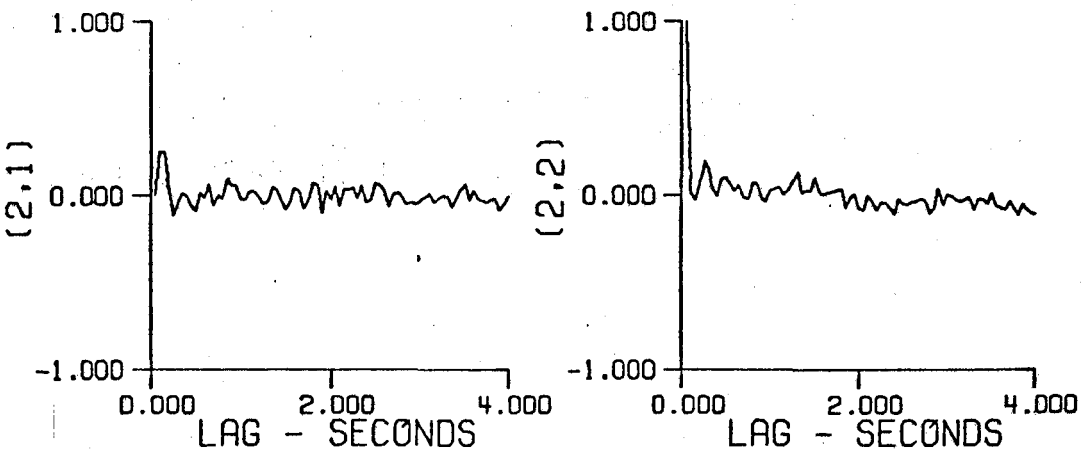
1.000
0.000
-1.000
(2,1)
0.000
2.000
4.000
LAG - SECONDS
1.000
0.000
-1.000
(2,2)
0.000
2.000
4.000
LAG - SECONDS

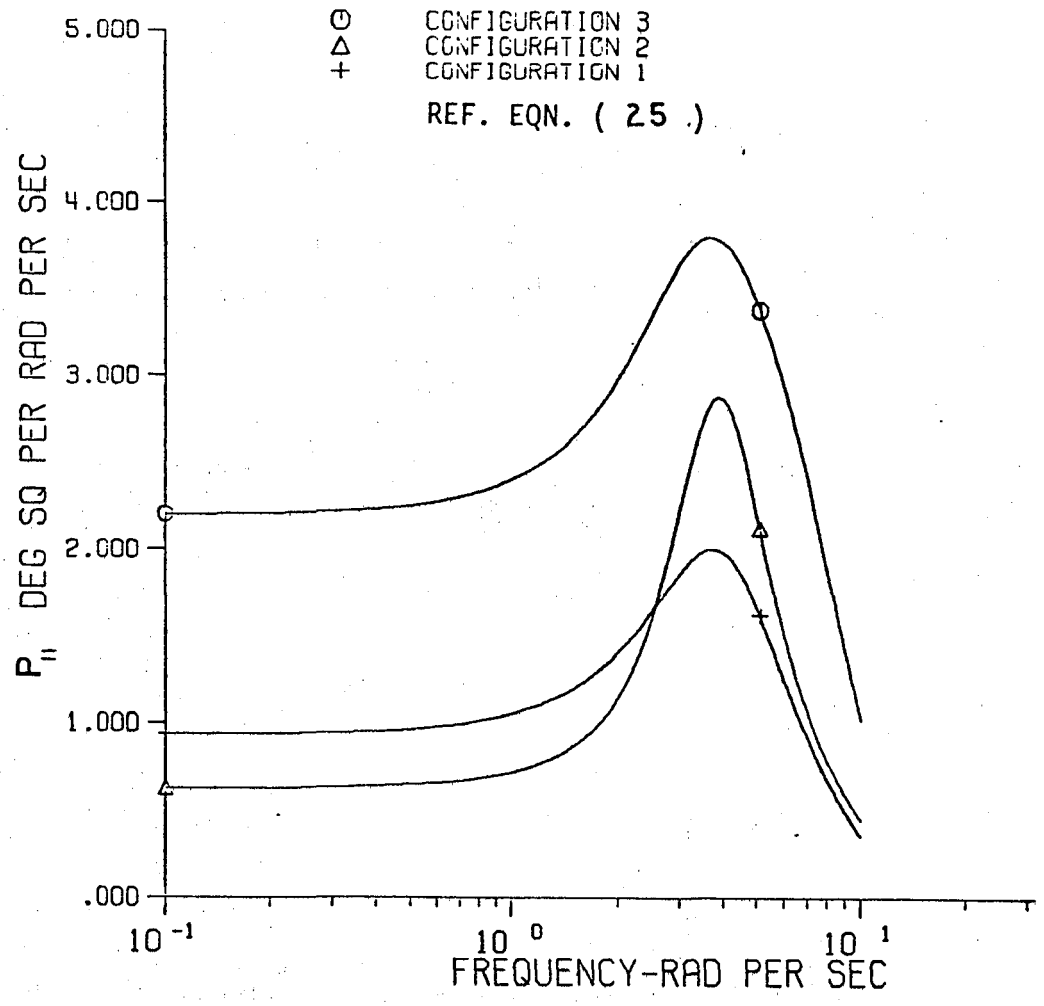
CONFIGURATION 3
CONFIGURATION 2
CONFIGURATION 1
REF. EQN. (25 .)
5.000
4.000
3.000
2.000
1.000
.000
P_{11} DEG SQ PER RAD PER SEC
10^{-1}
10^{0}
10^{1}
FREQUENCY-RAD PER SEC

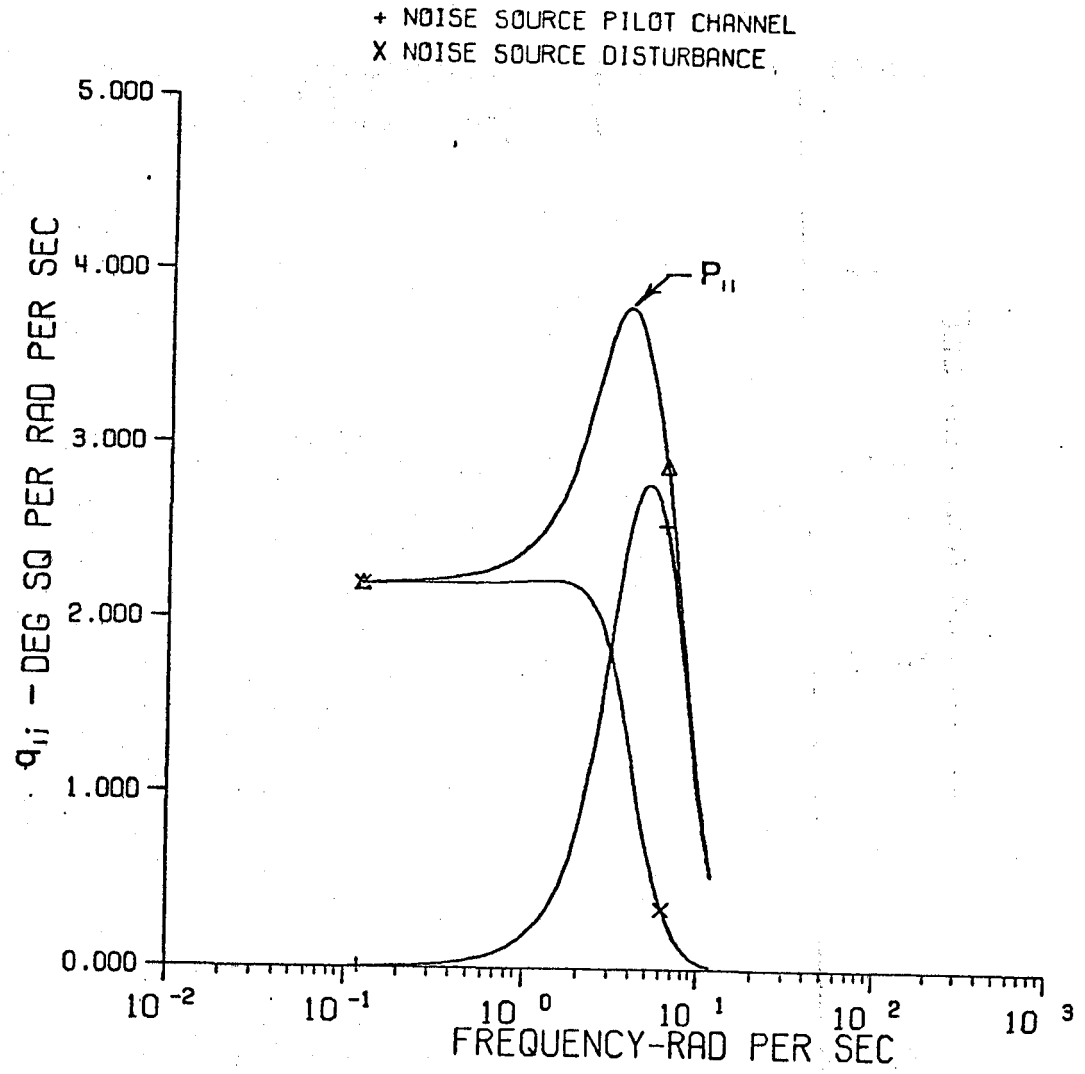
+ NOISE SOURCE PILOT CHANNEL
X NOISE SOURCE DISTURBANCE
5.000
4.000
3.000
2.000
1.000
0.000
q_{ij} - DEG SQ PER RAD PER SEC
P_{11}
10^{-2}
10^{-1}
10^{0}
10^{1}
10^{2}
10^{3}
FREQUENCY-RAD PER SEC

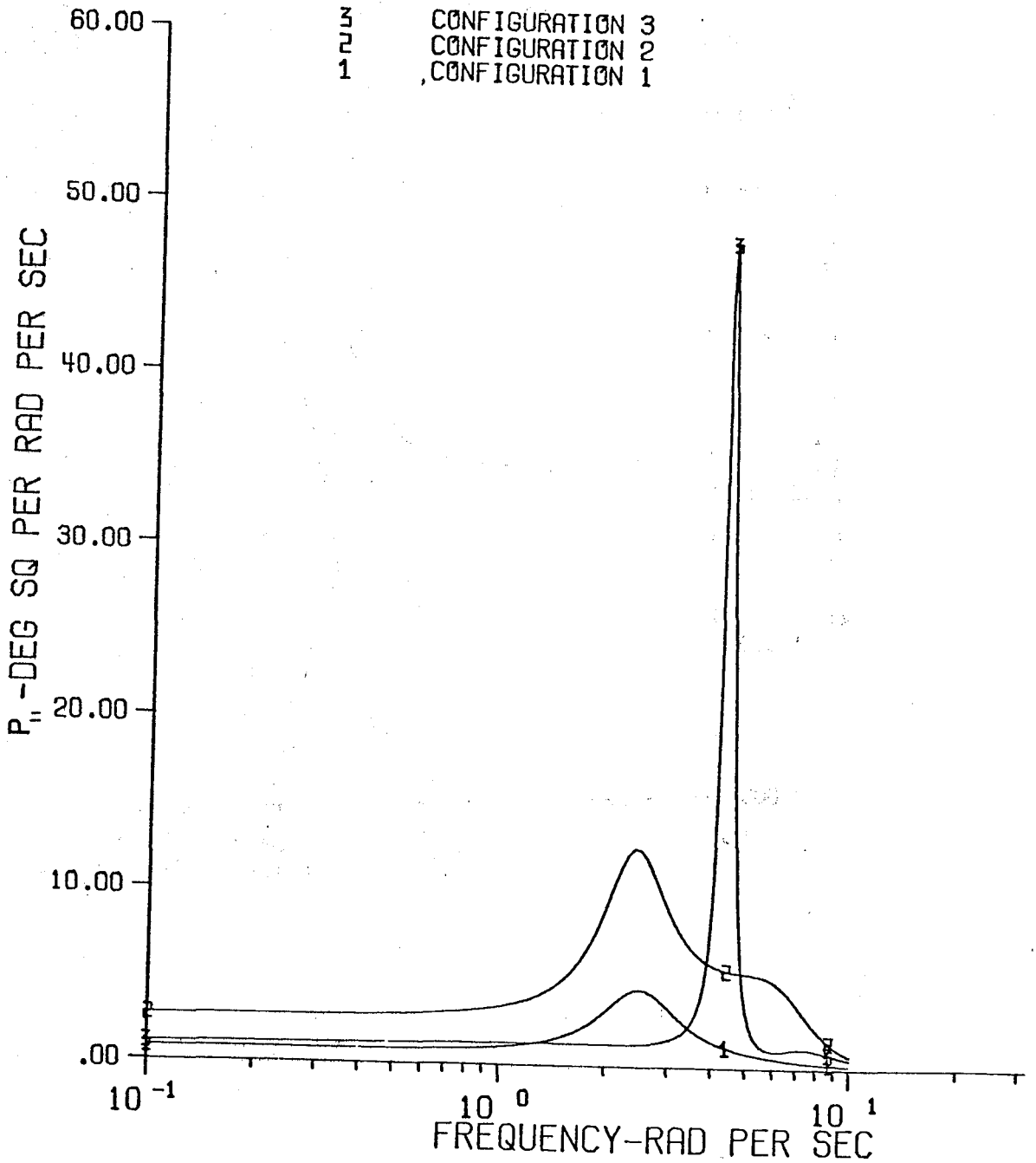
3 CONFIGURATION 3
2 CONFIGURATION 2
1 ,CONFIGURATION 1
60.00
50.00
40.00
30.00
20.00
10.00
.00
P_ii -DEG SQ PER RAD PER SEC
10 -1
10 0
10 1
FREQUENCY-RAD PER SEC

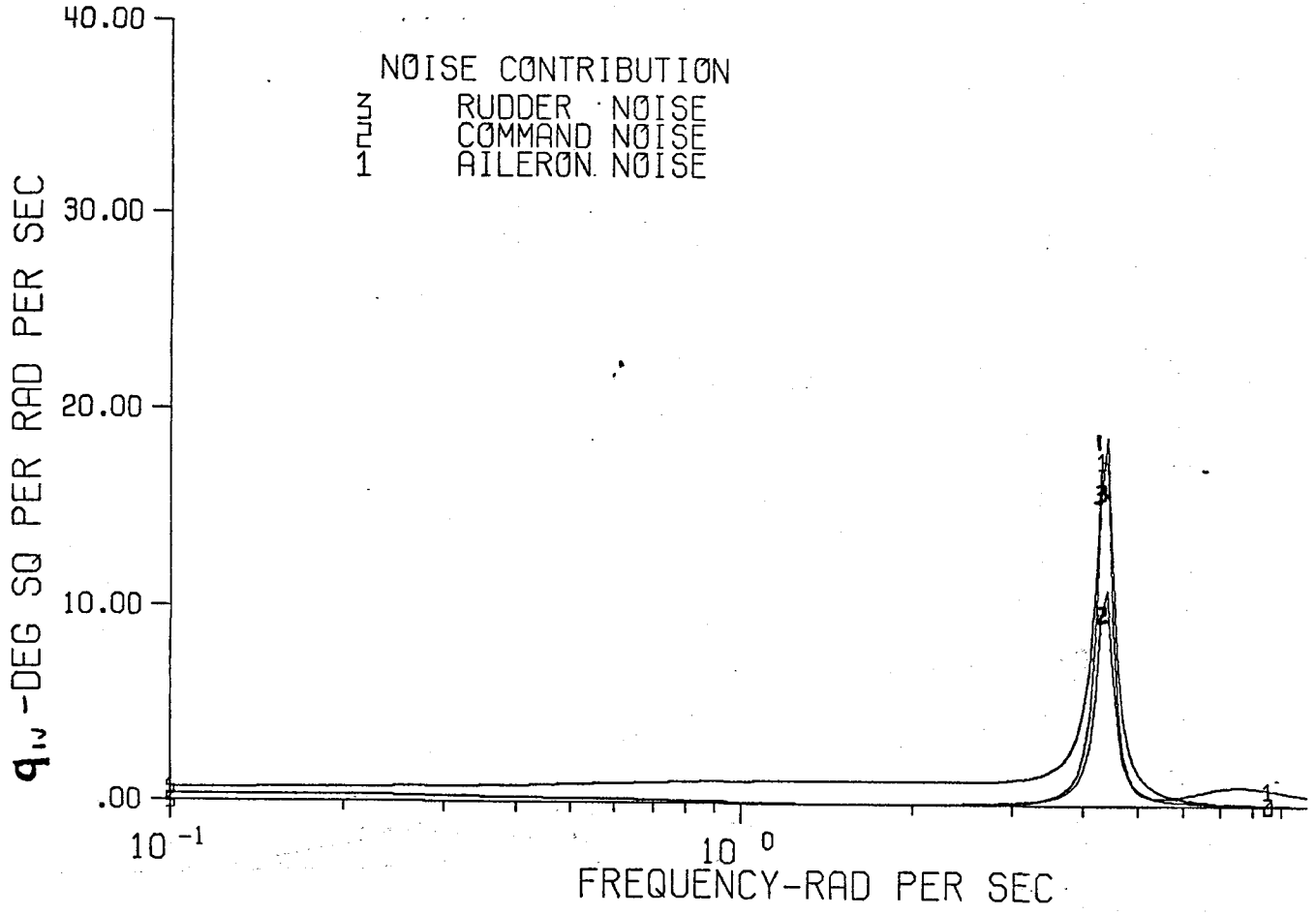
NOISE CONTRIBUTION
3 RUDDER NOISE
2 COMMAND NOISE
1 AILERON NOISE
40.00
30.00
20.00
10.00
.00
$q_{1,j}$ -DEG SQ PER RAD PER SEC
10^{-1}
10^{0}
FREQUENCY-RAD PER SEC

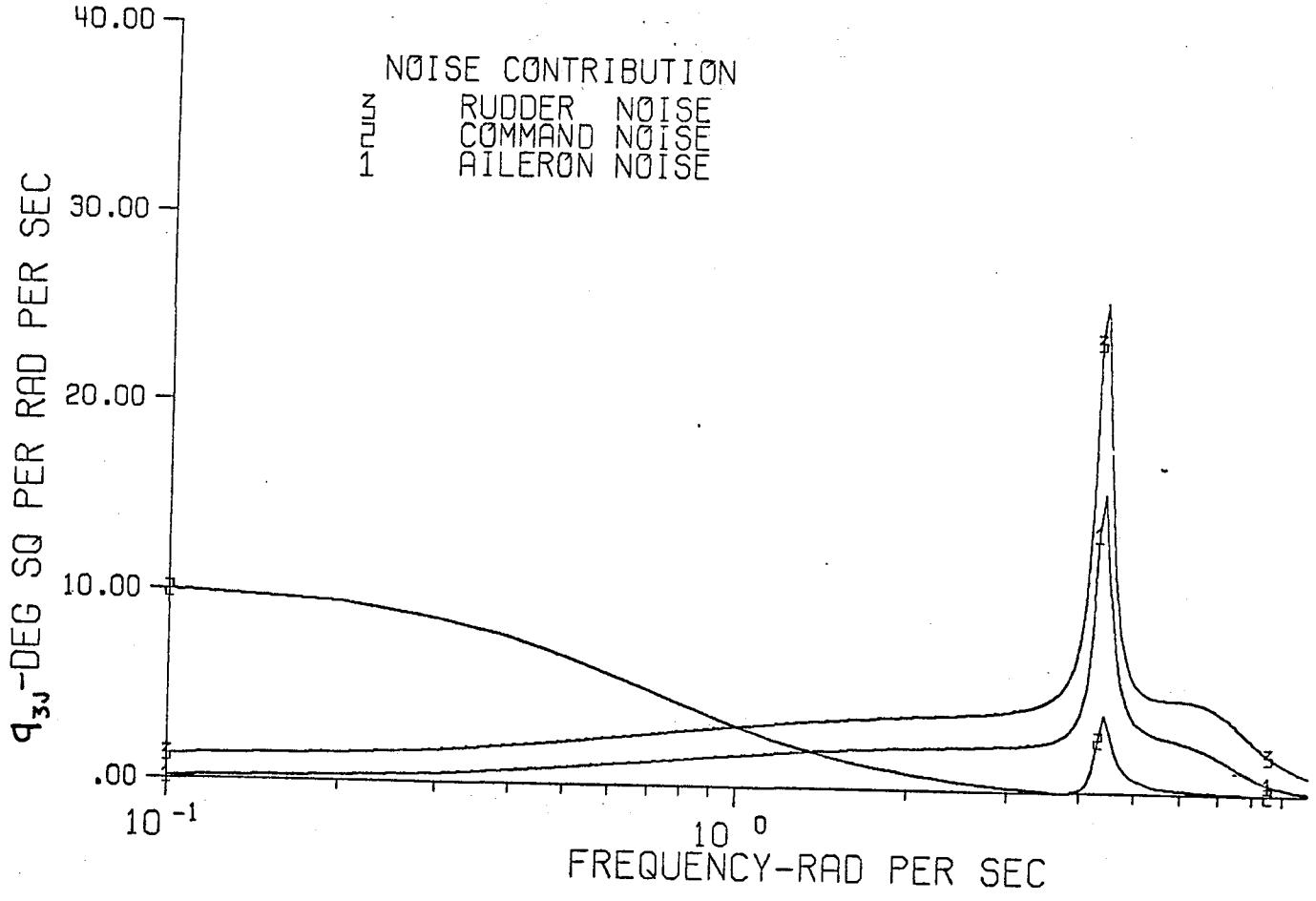
NOISE CONTRIBUTION
3 RUDDER NOISE
2 COMMAND NOISE
1 AILERON NOISE
40.00
30.00
20.00
10.00
.00
q_{3J}-DEG SQ PER RAD PER SEC
10^{-1}
10^{0}
FREQUENCY-RAD PER SEC

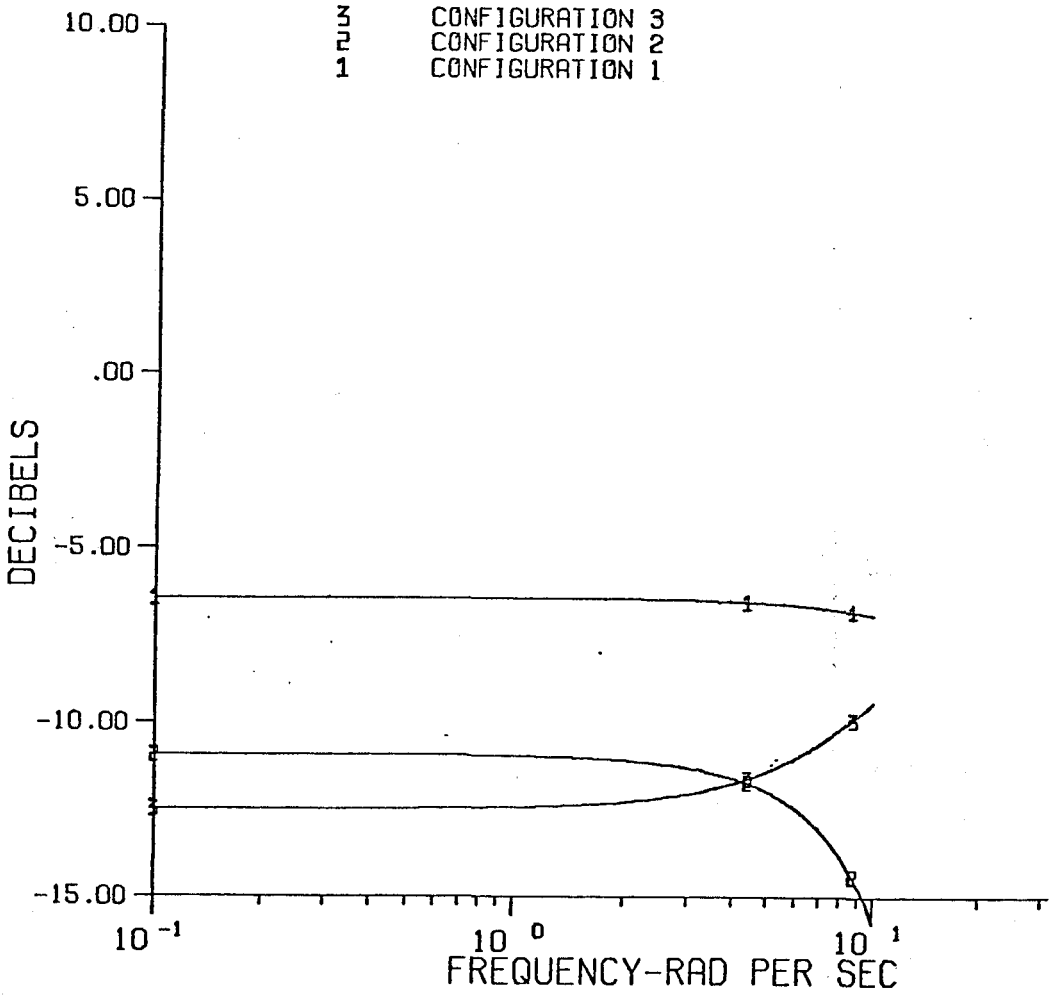
3 CONFIGURATION 3
2 CONFIGURATION 2
1 CONFIGURATION 1
10.00
5.00
.00
-5.00
-10.00
-15.00
DECIBELS
10 -1
10 0
10 1
FREQUENCY-RAD PER SEC

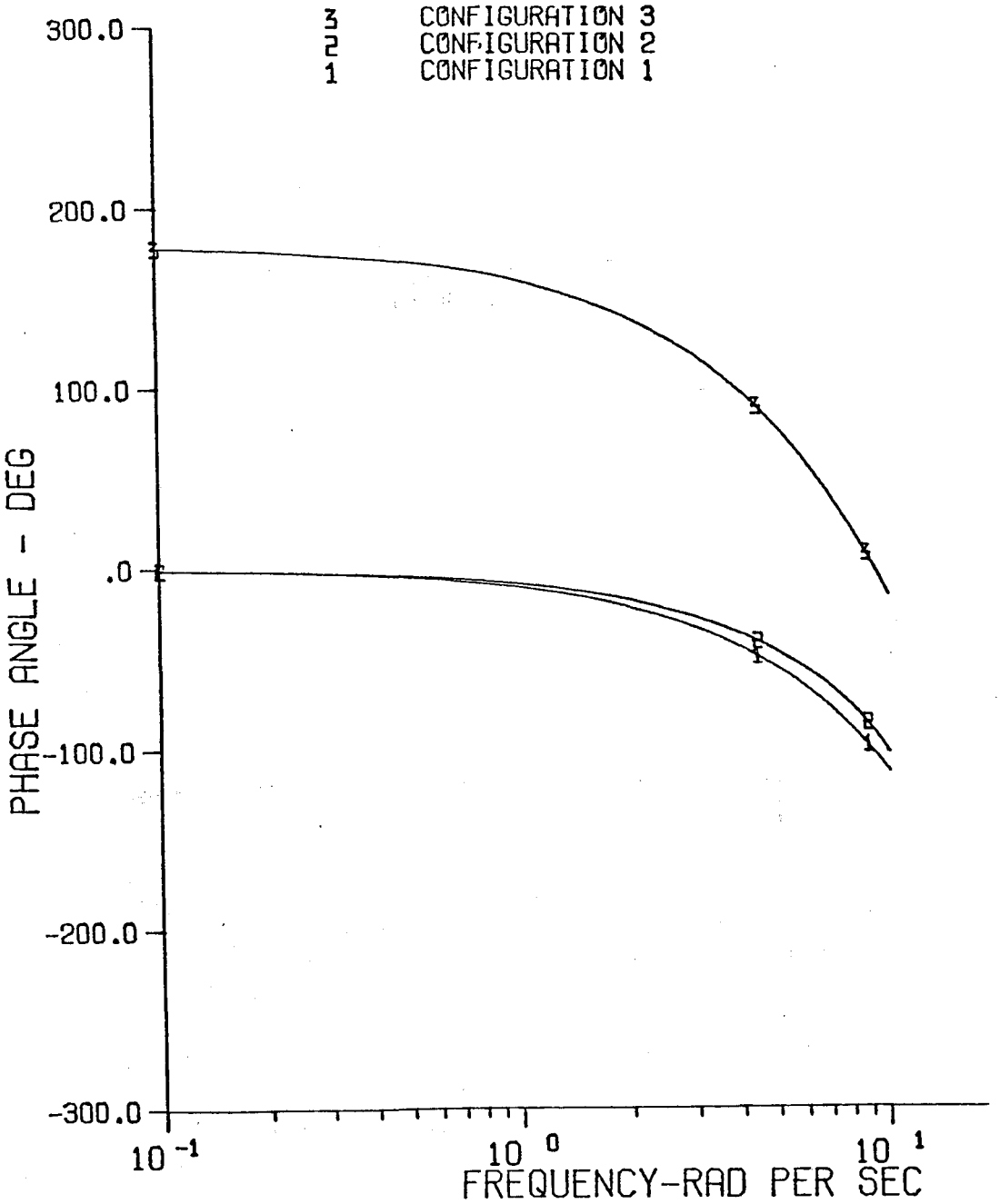
3 CONFIGURATION 3
2 CONFIGURATION 2
1 CONFIGURATION 1
300.0
200.0
100.0
.0
-100.0
-200.0
-300.0
PHASE ANGLE - DEG
10 -1
10 0
10 1
FREQUENCY-RAD PER SEC